Alumina-supported MoNx, MoCx and MoPx catalysts for the hydrotreatment of rapeseed oil

Jan Horáček, Uliana Akhmetzyanova*, Lenka Skuhrovcová, Zdeněk Tišler, Héctor de Paz Carmona

Unipetrol Centre for Research and Education, Block 2838, 436 70, Litvínov-Záluží 1, Czech Republic

ABSTRACT

The catalytic activity of molybdenum carbide (MoCx), nitride (MoNx), and phosphide (MoPx) was compared in the hydrotreatment of rapeseed oil performed in a continuous fixed bed reactor at 350–390 °C, 5.5 MPa and various Weight Hourly Space Velocities (WHSV). The deoxygenation activity was in the following order: MoCx > MoNx > > MoPx. In the case of MoCx, the temperature increase resulted in a decrease of the deoxygenation activity due to the competitive hydrocracking. Wherein, MoNx showed the highest tendency to hydrocracking and very strong effect of WHSV at 350 °C, which then became less significant at higher reaction temperatures. While MoPx activity was strongly influenced by the mass transfer limitations.

1. Introduction

The ever-increasing demand for transport fuel contributes the depletion of crude oil and a significant increase in pollutions resulting from its processing and utilization with inherent greenhouse-gases emissions. European legislation requires energy and CO_2 emission savings in industry and transportation. The demand for hydrocarbon-based materials for fuel production results in the large interest of producers in renewable feedstock and its effective conversion into automotive fuels. These renewable resources for alternative fuel production are typically lignocellulose- or triglyceride-based materials. Both feedstock types are supposed to be used for fulfilling European directives.

Lignocellulose (wood, straw, etc.) conversion into liquid fuels requires sophisticated industrial processes, like gasification followed by gas cleaning systems (tar, NH_3, H_2S, COS, HCN, HCl separation [1] and Fischer-Tropsch synthesis with hydroisomerization [2–8]). Another way to transform lignocellulosic biomass into fuels is its pyrolysis to bio-oil. Industrial scale processes for automotive fuels production from bio-oil have not been introduced yet. Bio-oil hydrodeoxygenation (HDO) is being widely investigated [9–18], but high technological difficulties and low process yields make the process perspectives challenging.

Vegetable oil hydrotreatment represents an attractive reaction for alternative fuel production, in particular renewable diesel components. The components are hydrocarbons occurring by hydrotreatment of unsaturated hydrocarbon chains, i.e. by the competitive deoxygenation by HDO or (hydro)decarboxylation/decarbonylation (HDC/HDCn) reaction pathways. Typically, a mixture of C_{15}-C_{18} n-alkanes represents the main product yielding around 80–85 wt.%, with 5 wt.% yield of light gases (C_3H_8, CH_4 and CO_x) and around 10–12 wt.% yield of water, depending on a feedstock origin, reaction conditions and catalysts used [19]. The main product with a cetane number of more than 60 may find application in diesel fractions blending as a cetane number booster. Possible deterioration of the cold flow properties could be easily overcome by the second step of isomerization of n-paraffins or addition of additives [20,21].

Conversion of vegetable oil was deeply investigated in the last decades, especially over conventional hydrotreating catalysts based on supported transition metal sulfides [22–24]. The reason for their use was given by advantage of the possibility to use already existing hydrotreating reactors and catalyst portfolios. The main difference in comparison to conventional hydrotreatment of middle distillates is given by high heat of reaction, around 1275 kJ/kg for pure soybean oil and 145 kJ/kg for fossil middle distillates, respectively [25]. Another specific parameter of this reaction is the hydrogen consumption of triglycerides deoxygenation reaching around 39.0 kg/ton for soybean oil and about 3.7 kg/ton in the case of conventional middle distillates [25]. These aspects bring limitations in processing of pure triglyceride feedstock and due to the limited hydrogen make-up and cooling gas/quench capacities. As an optimal way with adequate costs, co-processing of a maximum of 10 wt.% of triglycerides together with conventional feedstocks was proposed as a suitable way [26].

---

* Corresponding author.
  E-mail address: uliana.akhmetzyanova@unicre.cz (U. Akhmetzyanova).

The current development in the field of triglyceride transformation into hydrocarbons is given by the legislative pressure to minimize the sulfur content in the product to maximum 10 ppm as well as to increase the content of renewables in diesel fuel. As shown by Kubička [27] and proposed by Huber and co-workers [26], hydrotreatment of pure triglyceride feedstock requires a sulfur donor agent or H_2S dosing into the reactor, to avoid sulfur leaching from the catalyst active phase. The use of sulfur-free catalysts, in a tailored hydrotreating unit for the processing of triglyceride based feedstock, would represent the way for the production of 100% renewable materials for diesel oil blending with close to zero sulfur content. As possible catalytic materials, supported noble metal catalysts were investigated [13,14], as well as transition metal carbides, nitrides, and phosphides. Due to the typically high costs of noble metal catalysts, transition metals-based alternatives seem to be more perspective [28–33]. In the case of commercially used hydrotreating catalysts, the active phase is typically based on transition metals such as molybdenum, nickel, tungsten, cobalt and their combinations [32].

As bulk Mo_2C was found to be less active than supported Mo_2C [34] in conversion of stearic acid and fatty acids methyl esters as renewable model compounds, the supported catalysts are supposed to be developed. Studies of carbon-based catalyst supports, such as active carbon or carbon nanofibers [35] were presented showing high catalyst activity at temperatures starting at 240–280 °C and H_2 pressure 1.4–2.5 MPa. In the case of the carbon nanofiber support, Mo_2C active phase preferred HDO mechanism for oleic acid rather than decarboxylation and decarbonylation at hydrotreating reactions conditions commonly used in refineries (350 °C, 5.0 MPa) [36]. At the same conditions, W_2C active phase with the identical catalyst support showed lower hydrotreating activity accompanied by the more significant decarboxylation/decarbonylation reaction pathway, yielding a higher amount of olefins and heptadecane. In some specific cases, the production of lighter hydrocarbons might be preferred as triglyceride hydrotreating products. The carbide active phase was described as suitable for this type of conversion with NiMo bimetallic nature and ZSM-5 as a support, as well as the same analogy with the nitride active phase [37]. The same yields of organic liquids were described for both active phase types at different reaction temperatures. In this comparison, the carbide active phase showed little higher selectivity to gasoline. The Ni:Mo ratio of carbide active phase equal to 1:2 was found to be the best for the highest yields of liquid products. An increase of NiMo ratio results in a decrease in the overall yield of liquid products [37].

Comparison of the catalyst supports (400 °C, 4.5 MPa) showed [38] that over the carbide NiMo active phase the yields of organic liquid products were lower than 80 wt.% due to an intensive cracking when ZSM-5 or zeolite β was used as the catalyst support. On the other hand, SBA-15 and γ-Al_2O_3 showed the organic product yields over 90 wt.%. Despite the fact that it seems like a good result, such high yields were probably reached due to the incomplete deoxygenation degree under the used conditions. The USY catalyst support changed NiMoC activity to minor cracking, that was accompanied with the yield of the liquids around 85 wt.% at steady state with the diesel fraction being the main product.

The aim of this study is to compare activity of molybdenum nitride (MoNx), carbide (MoCx) and phosphide (MoPx) supported on γ-Al_2O_3 in the hydrotreatment of rapeseed oil. The reason for the catalyst support selection was made from the commercial point of view as the deoxygenation of triglycerides can be easily operated over γ-Al_2O_3 sulfided catalysts [39]. These catalysts represent a promising alternative to the conventional sulfur ones, allowing a high processing of vegetable oil, without the problems derived from the catalyst activity decrease. In the research scope, product quality and reaction mechanisms were evaluated as key factors for the further introduction of the alternative catalysts into industrial processes.

2. Experimental

2.1. Catalysts synthesis and characterization

MoCx, MoNx and MoPx supported on γ-Al_2O_3 were prepared by incipient wetness impregnation of a hexamethylenetetramine - ammonium heptamolybdate (HMT-AHM) precursor complex [40]. The first step was the preparation of the HMT-AHM complex using the method reported by Afanasiev [41]. The precursor complex was impregnated on γ-Al_2O_3 particles (224–560 μm) [42] and dried overnight at 120 °C. In the case of MoPx, the impregnated support was saturated with $(NH_4)_2HPO_4$ solution to obtain Mo:P ratio 1:1 (mol:mol) and dried again. The second step was the final transformation of the impregnated support to nitride, carbide or phosphide form by temperature-programmed reduction. The process was carried out in a tubular quartz reactor with a total length of 140 cm and the length of the heated zone of 100 cm. The reactor tube was located inside a three-zone electric heater controlled by PID regulators. A cuvette with the impregnated support was placed inside the quartz tube. The temperature program was set from ambient temperature to 200 °C in N_2 flow (10 °C/min, 75 cm^3/min) and from 200 to 700 °C (10 °C/min), and kept at 700 °C for 3 h under the synthetic gas flow (150 cm^3/min). A mixture of 20 vol.% of H_2 in N_2 was used for MoNx and MoPx preparation. MoCx was synthesized using 20 vol.% of CH_4 in H_2. After that, the reactor was cooled to the room temperature under the synthetic gas mixture flow, flushed with N_2 and the sample was passivated by a mixture of 1 vol.% of O_2 in Ar. All laboratory synthesized samples and the support were analysed using conventional physicochemical methods before catalyst activity testing.

The elemental composition of the samples was ascertained by inductively coupled plasma optical emission spectrometry (ICP OES) using Agilent 725. The samples were dissolved in sulfuric acid, then, the solution was fed to argon plasma. Merck standard solutions were used for calibration curves. The content of C and N in the samples was measured using elementary analyser Flash 2000 from Thermo. The standard for calibration was 2,5-bis (5-tert-butyl-2-benzooxazol-2-yl).

A crystallographic structure of the samples was determined by X-ray powder diffraction (XRD) patterns obtained on D8 Advance ECO (Bruker) applying CuK_{α} radiation (λ = 1.5406 Å). The step size of 0.02° and a step time of 0.5 s were used. The patterns were collected from 5° to 70° over the 2θ range and evaluated with the DIFFRAC.EVA V 4.1.1 software. The specific surface area (S_{BET}) was determined by N_2 adsorption/desorption at −196 °C using Autosorb iQ (Quantachrome Instruments) and Brunauer-Emmett-Teller equation (BET). Mercury (Hg) porosimetry measurements were performed on Micromeritics AutoPore IV 9510. Prior to both analysis, all samples were dried in a glass-cell at 200 °C under vacuum for 16 h. The morphology of the catalytic materials was examined by transmission electron microscopy (TEM) using JEM 1400 plus manufactured by JEOL. The analysis was performed in the acceleration voltage of 120 kV and the resolution of 0.98 nm for Quemsa II MPix bottom mounted digital camera. Air/oxygen stability of the prepared samples was studied by the thermogravimetric analysis (TGA) using TGA Discovery series (TA Instruments) operating at the constant 80 and 200 °C in an oxygen atmosphere (20 ml/min) for 8 h. The heating rate from 50 °C to the working temperature was set on 10 °C/min. The surface structure of the synthesized samples and their layout on the support were analysed by scanning electron microscopy (SEM). SEM images under 100 000x and 25 000x magnification were obtained using JSM-7500 F (JEOL Ltd.) with a cold cathode - field emission SEM (parameters of measurements: 1 kV, GB high mode). For deeper analysis under 5 000x magnification, samples were coated with about 5 nm of golden to make them conductive under the microscope (JEOL JSM-IT500HR) accessorized with energy-dispersive X-ray spectroscopy (EDS) for elemental analysis or map analysis. Representative backscattered electron or secondary electron images of microstructures were taken in high vacuum mode
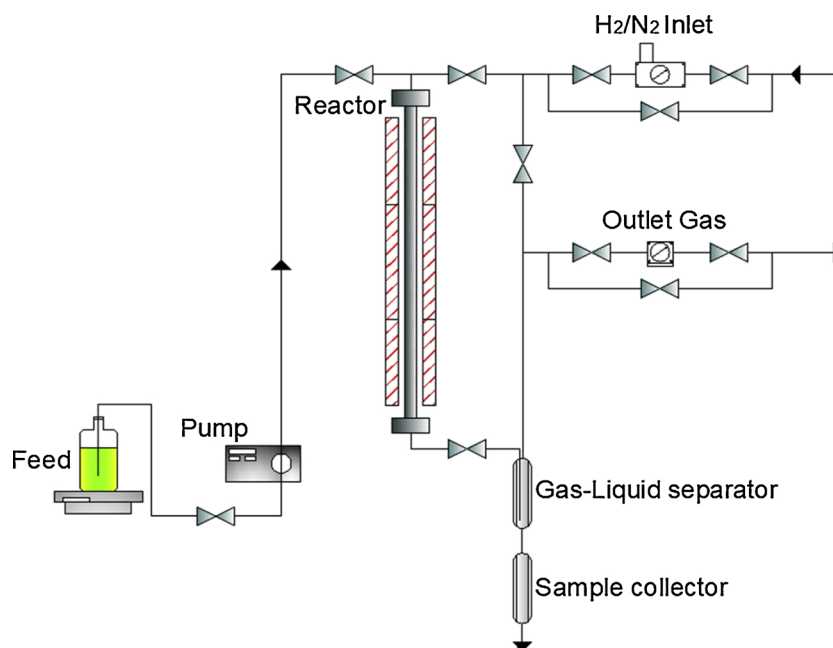
Fig. 1. The experimental setup.

using an accelerating voltage of 15 keV.

2.2. Experimental setup and characterization of products

Screening tests were carried out in a stainless steel tubular fixed bed reactor with an inner diameter 17 mm. To monitor the temperature profile of the reactor during the experiments, a 6 mm wide thermosonde sensor with six measuring points was placed in the middle of the reactor. The distance between the measuring points was 100 mm. The reactor tube was placed in a three-zone electric heating system with an independent controlling system for each segment. The experimental unit was equipped with two parallel pumps for the liquid feedstock (low or high flow) and Bronkhorst mass flow controller with the maximum flow of 600 N L/h. An overall pressure in the unit was controlled by a Kämmer control valve. Product samples were collected from a low-pressure separator. To avoid plugging of the product pipelines by saturated reaction intermediates, an additional trace heating system was installed to an original line (maximal temperature 100 °C). The experimental setup showed in Fig. 1 is placed in the experimental facility building of UniCRE in Litvínov-Záluží, Czech Republic.

Before each experiment, 10 g of the catalyst sample with the particle size of 224–560 μm was divided into four equal parts (2.5 g). Each part was mixed with the fine fraction (the particle size of 0.1 mm) of inert SiC to reach the catalyst:SiC (vol:vol) ratios of 1:1, 1:2, 1:3 and 1:4 using a graduated cylinder with a size similar to the diameter of the reactor. The bottom of the reactor was filled with inert SiC (the particle size of 1–2 mm). To stabilize the catalyst bed position, the plug of glass wool was placed on the top of the layer. The height of the SiC layer was calculated in order to place the catalyst bed in the centre of the heated zones of the reactor. Then the mixtures were loaded to the reactor layer by layer from high (catalyst:SiC 1:1) to lower (catalyst:SiC 1:4) catalyst concentration. In other words, the most diluted part was inserted to the top of the active layer and most concentrated - to the bottom. The concentration of the catalyst in the active layer was increased gradually in the direction of the reaction mixture flow, with the increasing conversion of the feedstock. This evokes the low conversion in the top of the catalyst bed, where the catalyst meets highly reactive feedstock. This catalyst loading method was developed to reduce local overheating of the reactor, which influences significantly on the vegetable oil HDO. The heat effect of the reaction pathways plays an important role due to

its value is 1144.2 kJ/mole for HDO mechanism and 1291.2 kJ/mole for decarboxylation with the total CO_2 reduction (data for triolein molecules, exact values depend on the vegetable oil origin and type). By this reason, it was possible to control the temperature profile with an accuracy of +/- 2 °C along with the catalytic layer during the reaction. Pure fine SiC (10 mL) was placed on the top of the catalyst bed as a gas and liquid distributor. The rest of the reactor volume was filled with inert SiC (the particle size of 1–2 mm). All the handing with the catalysts were performed under N_2 atmosphere.

After catalyst loading, the reactor was closed and the leak test was performed with N_2 pressure of 90 bar for 2 h. Then the reactor was flushed with H_2 under 2 bar and pressurized to 55 bar of H_2. The catalyst was treated under the H_2 flow 50 N l/h with the temperature heating rate of 20 °C/h to 450 °C. The final temperature was held for 4 h. After this procedure, the temperature along the catalyst bed was reduced to 350 °C and the H_2 flow was adjusted to 40 N L/h. Subsequently, pumping of the feedstock started with the flow rate of 20 g/h. Food quality rapeseed oil was used as the model feedstock to eliminate the deactivating effects of inorganic impurities, which were observed in the case of processing triglycerides over sulfided catalysts [27]. Reaction conditions were changed after stabilizing the product parameters (density at 20 °C, the refractive index at 20 °C). Each of the reaction temperatures (350, 370 and 390 °C) was combined with three levels of WHSV (1, 2 and 4 h^{-1}). The total H_2 pressure in the reactor was maintained at 55 bar throughout the experiment.

3. Results and discussion

3.1. Catalysts

All as-prepared samples were characterized by TGA to check their air/oxygen sensitivity at elevated temperatures (Fig. 2) due to the pyrolytic nature of the synthesized samples [43], and also to avoid the possible inefficiency of the passivation step. MoCx and MoNx had a mass loss of around 0.8 wt.% and 1.5 wt.% respectively at 80 °C. In both cases, the initial progressive mass loss took place before the gradual phase oxidation. Increasing the ageing temperature to 200 °C indicated that the MoCx phase was more sensitive to oxygen than MoPx and MoNx, while MoNx was found to be the most stable in this comparison. Based on these results, further handling of the samples was provided
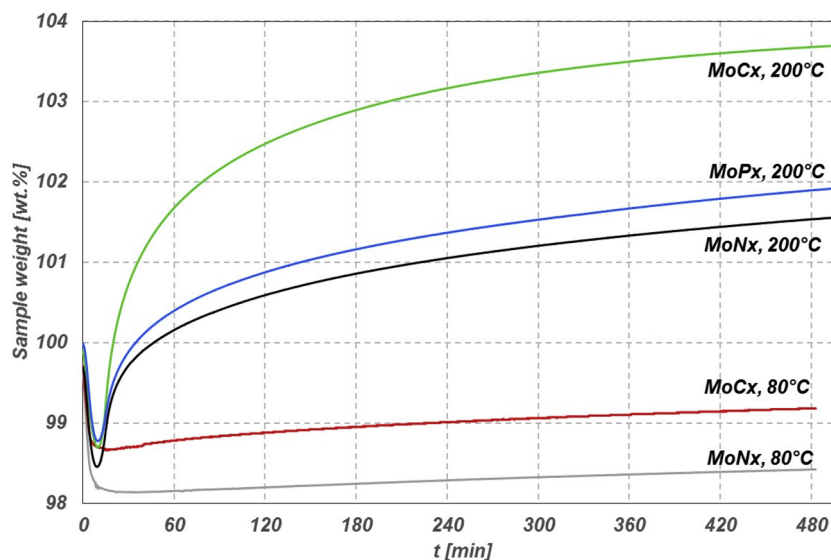
Fig. 2. TGA of the catalysts synthesized at 80 and 200 °C under O_2 atmosphere.

under inert atmosphere right after the synthesis until the loading to the experimental equipment.

Despite the claim that XRD is not suitable for characterizing Al-supported samples with low molybdenum loading [37], the technique was used to compare the phase composition and crystallinity of the synthesized materials. The XRD results pointed to low crystallinity with a dominant amorphous phase for all synthesized samples (Fig. 3) [40]. Based also on nitrogen and phosphorus content (Table 1), nanocrystallite or almost amorphous MoPx mainly consisted of aluminium oxide from the alumina support (PDF 80-1385); MoO_2 or Tugarovite ($2\theta = 26.0$, 37.0, 37.3; PDF 86-0135). The sample was characterised also by insignificant XRD signals of hexagonal and tetragonal mixed phosphide phases ($2\theta =$ around 43.0; PDF 24-0771, PDF 89-5111) and traces of molybdenum and aluminium nitride or oxynitride. As well as MoPx, MoNx had almost amorphous nature with presence of aluminium nitride and oxynitride. However, MoNx had a well dispersed molybdenum nitride crystalline phase consisting of a mixture of tetragonal Mo_2N ($2\theta = 37.7$, 43.2, 64.1; PDF 25-1368) and cubic Mo_3N_2 ($2\theta = 37.4$, 43.4, 63.1; PDF 89-3712). Similar to MoPx and MoNx, the MoCx sample was characterized with the presence of aluminium oxide (PDF 80-1385) provided by the support and main phase of well

dispersed orthorhombic Mo_2C ($2\theta = 34.3$, 38.0, 39.4, 61.6; PDF 71-0242).

Comparing to pure ɣ-Al_2O_3, MoCx and MoPx differed significantly in median pore diameter. The pore diameter of the support increased from 7.0 nm to 24.7 and 21.3 nm of final carbide and phosphide respectively (Table 1). The change may be caused by the high-temperature treatment at 700 °C, which is close to the phase-changing temperature of Al_2O_3 recrystallization from ɣ to δ-crystalline structure. The assumption that the phase of alumina was not change during the high temperature treatment was confirmed by XRD (Fig. 3) and TEM (Supporting Information). From XRD it is clearly seen that there was no phase transformation from ɣ to δ crystalline structure. From TEM there was no agglomeration during high temperature treating [44].

Another reason could be a high molybdenum loading (Table 1), which led the reconstruction of the support. Slight increase of the median pore diameter was observed also for MoNx, but this phenomenon was not as significant as in the case of MoCx and MoPx. The low S_{BET} together with the low volume of pores (3–56 nm) pointed to the presence of narrow pores of the phosphide sample.

SEM was used to study the morphology of the synthesized samples and their layout on the support with evaluation of the preparation
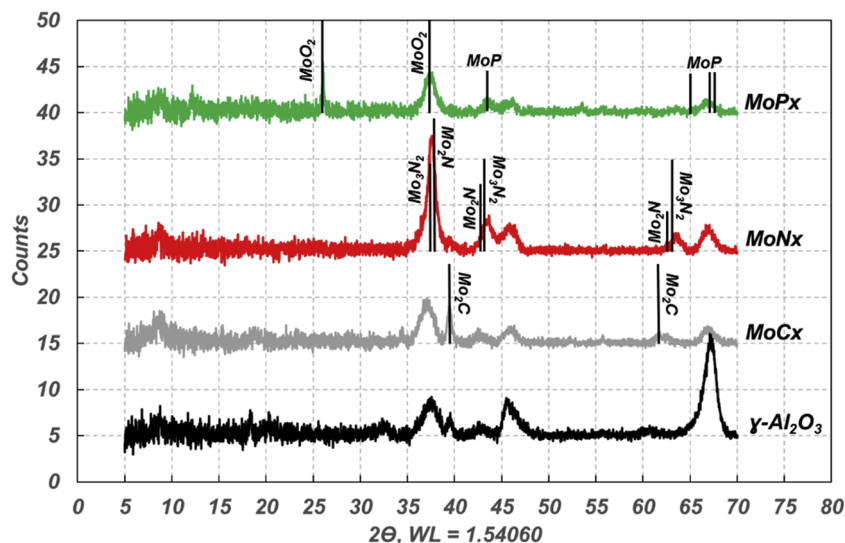

Fig. 3. XRD patterns of the MoCx, MoNx and MoPx catalysts supported on ɣ-Al_2O_3.

Table 1
Elemental and textural analysis of the support and synthesized samples.

Elemental analysis:		MoCx	MoNx	MoPx	γ-Al$_2$O$_3$
Fractions	Al	38.3	37.3	32.9	52.5
	Mo	22.1	21.3	19.8	-
[wt.%]	P	-	-	7.85	-
	N	-	0.85	0.52	-
	C	1.46	0.28	0.09	-
	Sum NCP*	1.46	1.13	8.46	-
Parameter:		Physical characterization			
S$_{BET}$ [m^2/g]		118.8	132.7	109.7	198.4
Total Intrusion Volume [mL/g]		1.35	0.55	1.05	0.77
Median Pore Diameter (Area) [nm]		24.7	9.3	21.3	7.0
Pore volume, 3-56 nm [mL/g]		0.49	0.51	0.31	0.75

[a]Sum of nitrogen, carbon and phosphorus contents.

method success. The resulted SEM microphotographs are in Supporting Information (Figs. S1–S3). SEM of MoCx showed the presence of two main structures on the surface. At high magnification (Fig. S1a), the amorphous/nanocrystalline phase was observed. Lower magnification (Fig. S1b) indicated a highly uniform surface and the presence of larger particles of about 0.2 – 0.5 μm. MoNx showed two significantly different structures on its surface. The first type is shown in Fig. S2a, c, where very fine structures can be found. To identify the nature of this surface structure, two explanations were proposed: (i) the areas could be formed by a thin layer of an amorphous molybdenum layer of MoNx covering alumina support, or (ii) these areas represent the original surface of γ-Al$_2$O$_3$ without any loading of the metal precursor or active phase. Based on the presence of bulky structures, the theory of uncovered alumina surface was preferred. The other type of the structures, located on the catalyst surface, was sponge-looking bulk particles (Fig. S2b, d) in μm size. These particles were determined by XRD as molybdenum nitride consisting of a mixture of tetragonal and cubic nitride phases (Fig. 3). The phosphide phase was better dispersed (Fig. S3a, b) than nitride, forming amorphous or nanocrystalline structures of a similar look to a carbide phase missing dominant particles as an observed in the case of the nitride phase.

To confirm the results, EDX at a lower magnification (5 000x) was provided. The analysis showed inhomogeneity of the samples (Fig. S4) in comparison to higher magnification results. The "islands" of molybdenum phases and the almost "pure" alumina porous support are clearly visible in the images. The analysis did not make possible to distinguish between the oxygen of the support, oxygen from tugarovite (MoO$_2$) or oxygen from any other mixed phases. Results of quantitative analysis obtained using SEM-EDX (Table S1) differ from the ICP OES results (Table 1). The difference in concentration of elements was reasoned by the fact that SEM-EDX is a "surface" analysis of a random sample area and ICP OES is a bulk analyses.

TEM was used as an additional method for investigating of crystalline structures of molybdenum carbide and nitride phase, as well as pure catalyst support before molybdenum loading. More detailed analysis and TEM microphotographs are moved to Supporting Information (Figs. S5–S8). The initial γ-Al$_2$O$_3$ (Fig. S5) showed an almost uniform structure formed from agglomerated alumina crystallites, including a small amount of pseudoboehmite detected by the presence of fibrous structures. The impregnation step did not affect crystallinity and led only to an uneven distribution of particle on the porous support (Fig.

S6) and the formation of polymer matrix covering the support particles.

3.2. Catalytic tests

The products collected at steady-state were analysed by the Simulated Distillation method (SIMDIS) and compared to describe hydrotreating and hydrocracking activities of the catalyst, as a function of reaction temperature and rapeseed oil WHSV.

3.2.1. The role of catalyst type

In order to analyse the catalyst activity, four main fraction yields were monitored in the liquid samples: naphtha (50–180 °C), middle distillate (180–360 °C), vacuum oil (360–550 °C) and residues with a boiling point (BP) of over 550 °C. The direct comparison of the catalysts (Fig. 4) at the same reaction temperature (350 °C) indicated that the highest yield of diesel-like products was between 73 and 80 wt.% of the product mass over the molybdenum carbide phase, which is in concordance with the results published by H. Wang and co. [38]. In fact, molybdenum carbide always showed high yield of the diesel-like fraction, as well as after increase of WHSV from 1 to 4 h^{-1}. Whereas, molybdenum nitride gave a linear fall of the diesel-like fraction compensated by heavier fractions. In the same way, the phosphide phase showed the lowest activity [45], producing the heaviest fraction as the main product. Moreover, the catalyst activity was not affected by WHSV changes and almost a constant product composition was obtained.

The increase in the yield of middle distillate at higher WHSV cannot be explained by a decrease in cracking activity due to very low naphtha yields at main WHSV (1 h^{-1}, Fig. 4a). This behaviour was given by incomplete deoxygenation of the feedstock resulting in fatty acids formation with BP in the range of middle distillate (Fig. 5) as shown by simulated distillation curves (Fig. 6a). Although, derivative SIMDIS analysis did not confirm any significant changes in the single peak intensities (Fig. 6b).

Significant changes in the product distribution on MoNx (Fig. 6c) were caused by the changes in WHSV, which could be related to a lower catalyst activity, attending to the not pure nitride phase in the catalyst. In this sense, the activity of nitride catalysts depends on several factors such as the metal oxidations state, N deficiency or anionic vacancies [32]. The changes in products distribution were appreciated as a gradual increase of the free fatty acid content (BP between 350–375 °C,
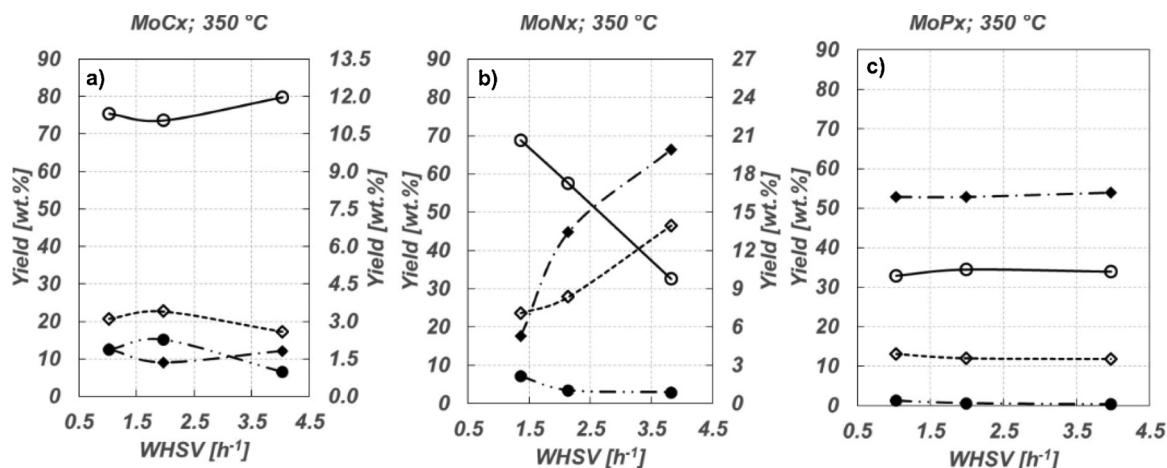
Fig. 4. Yields of the main product fractions from the rapeseed oil deoxygenation over the γ-Al$_2$O$_3$ supported MoCx (a), MoNx (b) and MoPx (c) catalysts at 350 °C and various WHSV. ● 50–180 °C; ○ 180–360 °C; ◊ 360,550 °C; 550 °C+. Full symbols related to the secondary Y axis.

Fig. 6d) and intermediate products represented by long chain esters (BP 475–520 °C). These values did not correlate with the real BP of stearyl stearate, which was identified as the main long-chain ester. This difference was attributed to the calibration method using the n-paraffinic calibration curve which is not ideal for oxygen-containing compounds.

Molybdenum phosphide, as the least active catalyst, showed a slightly decreasing tendency in the hydrocarbons formation and the minimal formation of acids and long-chain esters (fatty acid-fatty alcohol). The vacuum oil fraction and residue were represented typically by diglycerides and triglycerides or diacyl esters of propanediols respectively when gradual hydrogenolysis (Fig. 5) to fatty acids was taken into account. The absence of long chain esters and fatty acids was caused by mass transfer limitations given by worse accessibility of active centres for di- and triglycerides, while fatty acids can more easily penetrate narrow pores and turn into hydrocarbons. The worst availability of active centres can be explained by the location of the active phase in pores mouths, causing a bottleneck, or by clogging the catalyst pores, which leads to a decrease in the mass transfer rate. This partially explains the lower S$_{BET}$ (Table 1) as well as low volume of pores with diameter of 3–56 nm. A relatively high value of the average pore diameter was probably given by structures close to the outer surface of the catalyst particles.

3.2.2. The role of reaction conditions

The reaction temperature was investigated for each type of catalyst independently, however, the basic conclusions shown in Figs. 4 and 6 are generally valid. In the same way, MoCx showed the highest activity, MoNx - the medium activity and MoPx - the lowest activity in rapeseed oil catalytic deoxygenation, especially at the higher reaction temperature.

As generally known, an increase in the reaction temperature of hydrotreating reactions typically causes higher activity in oxygenates treating [46]. In this case, all the catalysts showed an identical decrease

in the deoxygenation activity after the reaction temperature was increased to 370 and 390 °C, respectively (Figs. 7–9).

As the most active, molybdenum carbide showed a high deoxygenation efficiency being selective at 350 °C mainly to products of HDO reaction pathway [28,47], i.e. n-hexadecane and n-octadecane. This fact means the promotion of HDO pathway in detriment of HDC/HDCn pathways (Fig. S9) [48]. The increase in WHSV resulted in a little decrease of deoxygenation degree accompanied by the presence of fatty acids in the product (Fig. 7a, d). The reaction temperature increase to 370 °C dramatically changed catalyst activity and selectivity. Similar to conventional sulfured catalysts [49], the long contact time by WHSV $= 1 \, h^{-1}$ in combination with 370 °C significantly promoted hydrocracking activity of catalyst producing higher contents of C$_{10}$-C$_{15}$ hydrocarbons (BP 175–270 °C). Moreover, cumulative SIMDIS (Fig. 7b) pointed to the decrease in the yields of compounds with the BP below 550 °C. This can be explained by a decrease of triglycerides deoxygenation due to its competitive nature with hydrocracking reactions, which are getting preferred due to the higher mobility of reactants, analogous to the effect observed by F. Wang over Mo$_2$C/AC catalysts during vegetable oil hydrotreatment [29]. Lower deoxygenation activity was confirmed by an increase in the concentration of fatty acids propyl esters (BP 400–420 °C). On the other hand, the selectivity to hydrocracking was reduced by higher WHSV. The gradual increase of WHSV to $2 \, h^{-1}$ and $4 \, h^{-1}$ caused the increase of compounds distillable to 550 °C by units of wt.% and reduced concentration of hydrocracking products. Another increase of reaction temperature to 390 °C, resulted in deeper cracking and higher naphtha yields, especially at WHSV $= 1 \, h^{-1}$, lower yields of middle distillate fraction and the more intensive formation of fatty acids propyl esters (Fig. 7f). The overall yield of products with the BP up to 550 °C reached 93 wt.% independently on WHSV (Fig. 7c).

The nitride phase showed the highest sensitivity of BP product distribution to WHSV at 350 °C (Fig. 8a, d). This fact was observed
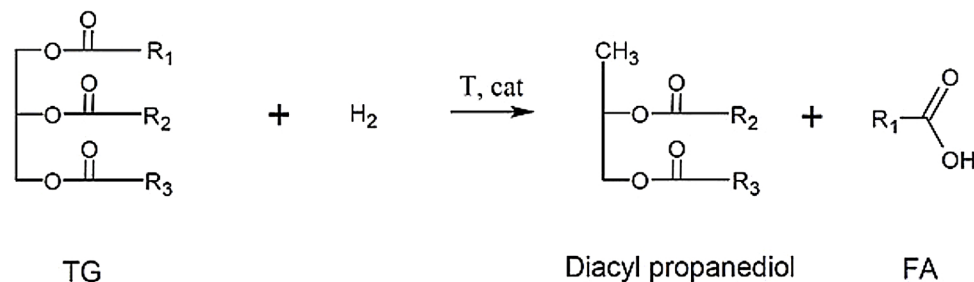

Fig. 5. Partial hydrogenolysis of the triglyceride structure (TG) into fatty acids (FA).
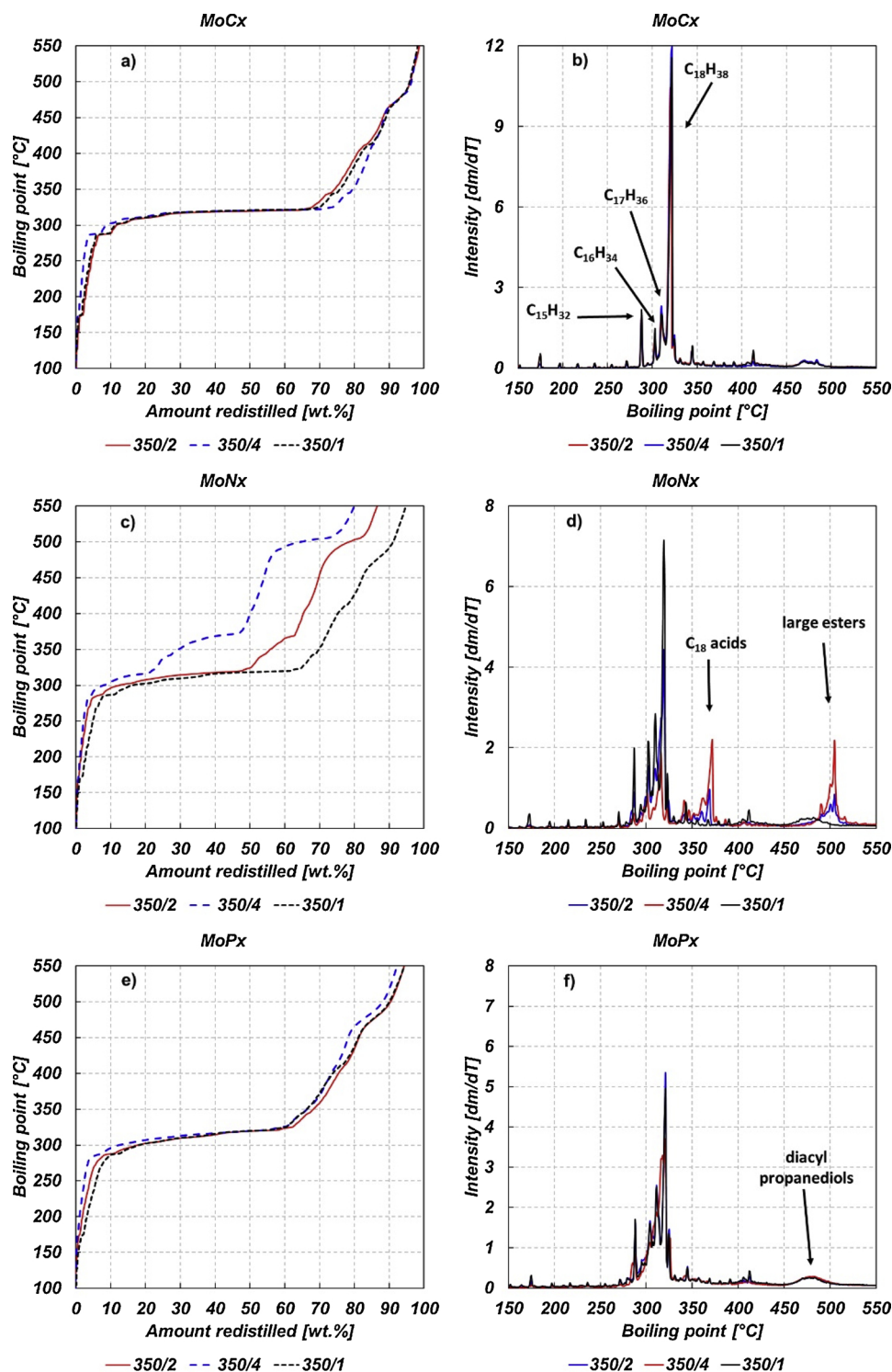
Fig. 6. SIMDIS analysis of the products of the rapeseed oil deoxygenation over the molybdenum carbide, nitride, and phosphide at 350 °C, WHSV = 1, 2 and 4 h^{-1}.

during the WHSV increase from 1 h^{-1} to 2 h^{-1}, which resulted in lower yields of hydrocarbons and in the presence of oxygen-containing intermediates in products, such as free fatty acids and their esters with fatty alcohols (long chain esters). These oxygenates became the main product after another WHSV increase to 4 h^{-1} (Fig. 8b, e). Both deoxygenation and hydrocracking reactions were promoted by reaction temperature increase to 370 °C. Especially short n-alkanes as hydrocracking products were detected by SIMDIS analysis for WHSV = 1 and 2 h^{-1}. At these conditions, the yield of the products, distillable till 550 °C, reached 90 wt.% and 86 wt.% at WHSV = 4 h^{-1}. It shows the

promoting effect of the reaction temperature to deoxygenation [46]. Moreover, at the highest WHSV, the content of naphtha components was significantly reduced. Hydrocracking activity becomes more significant than in the case of MoCx after the temperature increase to 390 °C. The yield of distillable products over 90 wt.% (Fig. 8c, f) indicated a high triglyceride conversion. At the same time, fatty acid propyl ester was obtained for all used WHSV. The yield of naphtha from 7 to 11 wt.% can be attributed also to hydrocracking of acyl groups of triglycerides and their hydrogenolysis intermediates.

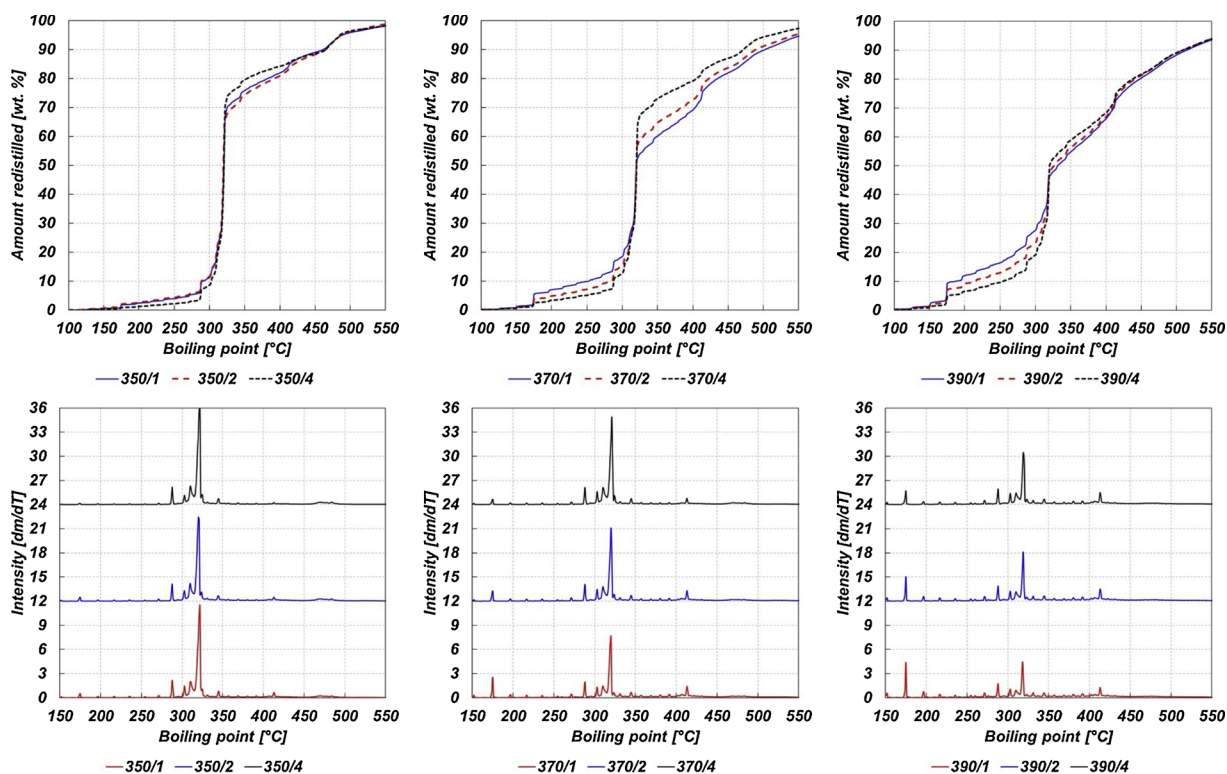Low hydrocracking activity and high yields of C$_{15}$-C$_{18}$ hydrocarbons

Fig. 7. Cumulative SIMDIS (a–c) and derivative SIMDIS of the rapeseed oil deoxygenation products catalysed by **MoCx** at temperatures 350 °C (a,d), 370 °C (b,e) and 390 °C (c,f) and WHSV = 1, 2 and 4 h^{-1}.
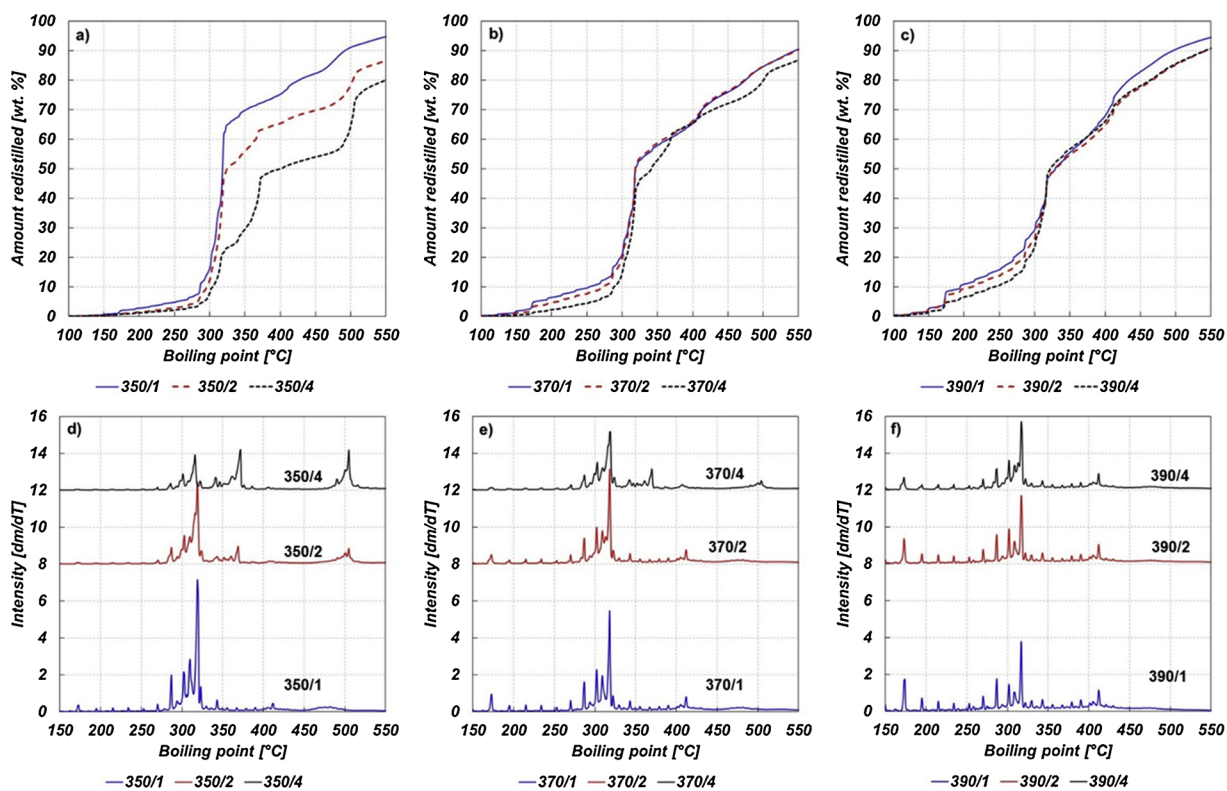

Fig. 8. Cumulative SIMDIS (a–c) and derivative SIMDIS of the rapeseed oil deoxygenation products catalysed by **MoNx** at temperatures 350 °C (a,d), 370 °C (b,e) and 390 °C (c,f) and WHSV = 1, 2 and 4 h^{-1}.

were typical for deoxygenation products over MoPx catalyst [47]. Unlike MoNx and MoCx, the increase of WHSV over phosphide phase at 350 °C did not evoke any changes in deoxygenation activity. The main change in product quality, in this case, was the range widening of C$_{15}$-C$_{18}$ n-alkanes (270–325 °C) and relatively lower peak intensities (Fig. 9a, d) which may be due to the different nature of these products.
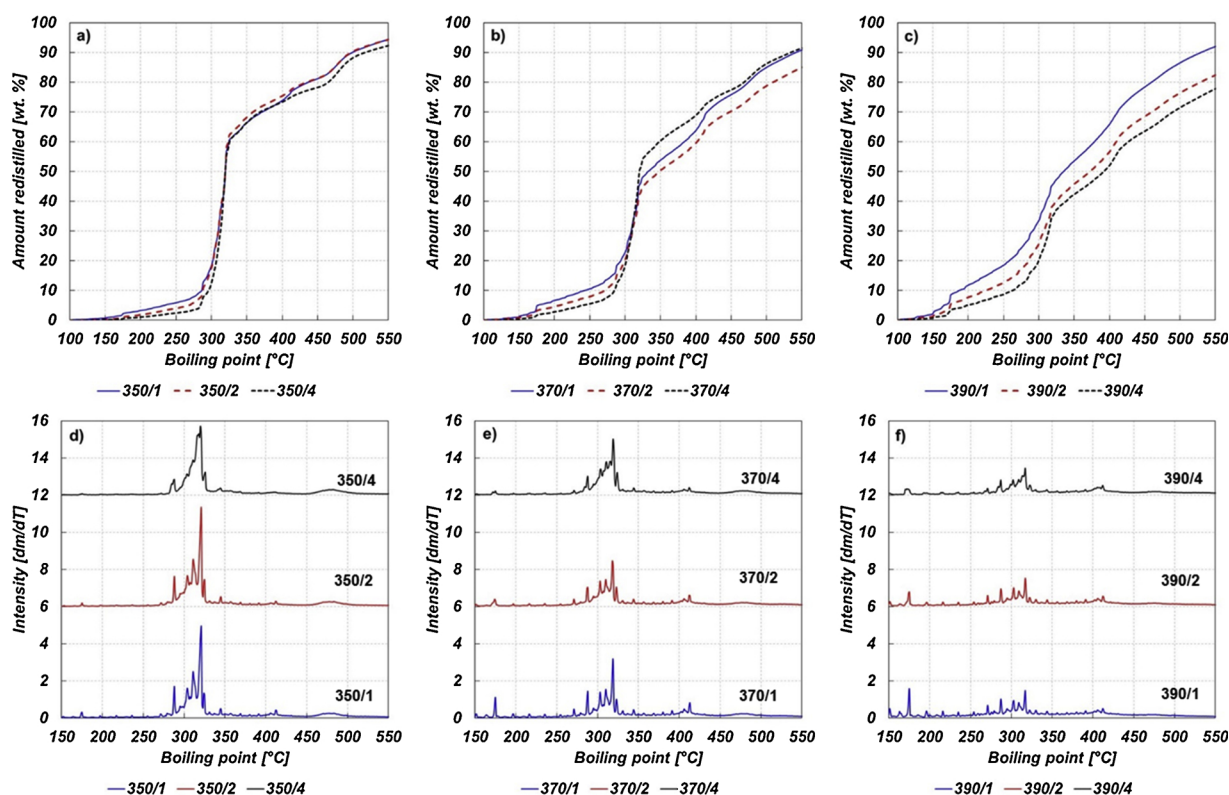
Fig. 9. Cumulative SIMDIS (a–c) and derivative SIMDIS of the rapeseed oil deoxygenation products catalysed by **MoPx** at temperatures 350 °C (a,d), 370 °C (b,e) and 390 °C (c,f) and WHSV = 1, 2 and 4 h^{-1}.

Typically, it corresponds with the presence of olefins and isoparaffins appropriate to the typical n-alkanes of this range.

Hydrocracking activity of the phosphide catalyst was found to be highly sensitive to the reaction temperature and WHSV, as an increase of temperature to 370 °C strongly promoted n-decane formation. Competitive nature of hydrocracking and deoxygenation reactions is responsible for hydrocracking inhibition at elevated WHSV (Fig. 9b, e). The lower yield of products distillable till 550 °C (84 wt.%, Fig. 9b) was probably caused by wrong handling with the sample causing loss of solid long chain esters. Following temperature increase to 390 °C, intensified hydrocracking of alkanes into C_8-C_{12} hydrocarbons and slowed down deoxygenation of triglycerides and diacyl propanediols, as showed by decreased yields of distillable products with the BP below 550 °C (Fig. 9c, f).

3.2.3. Gaseous products

Despite the fact that the liquid hydrocarbons are the main desired products, significant amounts of by-products were usually produced by triglyceride deoxygenation [50]. Gaseous products were represented by propane, which is a high added value residue of glycerol part of triglycerides, carbon oxides (CO_x) and methane. In the case of hydrocracking reactions occurrence, also other light hydrocarbons were formed, as it is the case of ethane and C_{4+} compounds.

In all the performed experiments, no carbon monoxide was detected in the off-gas stream (Table 2). At 350 °C, methane from CO_x reduction and propane were the main gaseous products. In general, it can be argued that increasing the reaction temperature leads to higher hydrocracking activity, which is according to the results described previously. This provides a more intense formation of light products (mainly C_2H_6) and an increase of C_{4+} compounds in the off-gas. On the other hand, an increase in the feedstock flow rate resulted in a decrease in methane content or formation, which is probably due to a lower deoxygenation rate.

Table 2

Relative distribution of gaseous products from each reaction conditions setup (only products without hydrogen).

MoCx	350 °C			370 °C			390 °C		
WHSV [h^{-1}]	1	2	4	1	2	4	1	2	4
C. dioxide [wt.%]	2.1	5.6	4.7	2.9	5.0	6.8	2.8	6.6	7.1
Methane [wt.%]	29.0	25.6	23.3	24.8	23.9	23.0	29.9	27.4	19.4
Ethane [wt.%]	2.8	2.7	2.2	4.1	3.4	2.9	6.9	5.7	3.7
Propane [wt.%]	56.2	60.2	61.1	47.7	49.2	53.0	26.7	37.1	37.5
C_{4+} [wt.%]	10.0	5.9	8.7	20.5	18.4	14.4	33.8	23.2	32.3

MoNx	350 °C			370 °C			390 °C		
WHSV [h^{-1}]	1	2	4	1	2	4	1	2	4
C. dioxide [wt.%]	10.9	11.2	10.8	18.2	12.0	12.7	16.5	15.4	11.9
Methane [wt.%]	23.8	20.1	22.7	12.3	21.0	17.2	24.7	19.2	19.2
Ethane [wt.%]	2.4	1.8	1.3	3.4	2.7	2.0	6.0	4.2	3.4
Propane [wt.%]	49.9	56.1	55.5	43.9	39.0	49.7	23.8	28.9	30.8
C_{4+} [wt.%]	13.0	10.8	9.6	22.2	25.3	18.4	29.0	32.3	34.8

MoPx	350 °C			370 °C			390 °C		
WHSV [h^{-1}]	1	2	4	1	2	4	1	2	4
C. dioxide [wt.%]	7.3	7.9	7.9	12.6	14.2	10.5	21.7	17.0	14.8
Methane [wt.%]	37.2	32.0	35.9	27.3	28.0	28.2	22.2	22.2	20.5
Ethane [wt.%]	2.7	2.8	2.1	4.0	3.6	2.8	6.4	4.9	3.3
Propane [wt.%]	36.2	43.0	40.1	30.5	31.0	37.9	18.9	22.1	21.5
C_{4+} [wt.%]	16.7	14.3	13.9	25.6	23.2	20.5	30.8	33.9	39.9

4. Conclusions

Hydrotreatment of rapeseed oil over molybdenum carbide, nitride and phosphide phases under identical reaction conditions showed differences in catalytic properties. The carbide phase was most active at

350 °C when producing n-paraffins with minor tendencies to hydro-cracking. Increases in the reaction temperature evoked a gradual loss of the deoxygenation activity due to the hydrocracking of paraffins into shorter chains. Similar behaviour was observed also on nitride and phosphide phases. The molybdenum nitride phase was selective to hydrocracking at 370 °C and to (hydro)deoxygenation at 350 °C with its strong sensitivity to the rapeseed oil WHSV. The molybdenum phosphide phase was less active in this comparison. Mass transfer difficulties inside the molybdenum phosphide catalyst resulted in a significantly lower deoxygenation activity and following deoxygenation products hydrocracking with increasing selectivity with raising the temperature.

Declaration of Competing Interest

The authors declare that they have no known competing financial interests or personal relationships that could have appeared to influence the work reported in this paper.

Acknowledgements

References

[1] P.M. Maitlis, A. de Klerk, Greener Fischer-Tropsch Processes for Fuels and Feedstocks, (2013), https://doi.org/10.1002/9783527656837.

[2] C. Bouchy, G. Hastoy, E. Guillon, J.A. Martens, Fischer-Tropsch waxes upgrading via hydrocracking and selective hydroisomerization, Oil Gas Sci. Technol. 64 (2009) 91–112, https://doi.org/10.2516/ogst/2008047.

[3] G. Pölczmann, J. Valyon, Á. Szegedi, R.M. Mihályi, J. Hancsók, Hydroisomerization of fischer-tropsch wax on Pt/AlSBA-15 and Pt/SAPO-11 catalysts, Top. Catal. 54 (2011) 1079–1083, https://doi.org/10.1007/s11244-011-9728-4.

[4] Y. Liu, K. Murata, K. Sakanishi, Hydroisomerization-cracking of gasoline distillate from Fischer-Tropsch synthesis over bifunctional catalysts containing Pt and heteropolyacids, Fuel 90 (2011) 3056–3065, https://doi.org/10.1016/j.fuel.2011.05.004.

[5] H.W. Schablitzky, J. Lichtscheidl, K. Hutter, C. Hafner, R. Rauch, H. Hofbauer, Hydroprocessing of Fischer-Tropsch biowaxes to second-generation biofuels, Biomass Convers. Biorefinery. 1 (2011) 29–37, https://doi.org/10.1007/s13399-010-0003-x.

[6] A. Galadima, O. Muraza, Hydroisomerization of sustainable feedstock in biomass-to-fuel conversion: a critical review, Int. J. Energy Res. 39 (2015) 741–759, https://doi.org/10.1002/er.

[7] L.A. Krasilnikova, A.I. Grudanova, L.A. Gulyaeva, Isodewaxing catalyst for processing of middle distillate fractions obtained from oil and Fischer-Tropsch synthesis products mixture, Catal. Commun. 98 (2017) 30–33, https://doi.org/10.1016/j.catcom.2017.05.001.

[8] L.C. Gomes, D. de Oliveira Rosas, R.C. Chistone, F.M.Z. Zotin, L.R.R. de Araujo, J.L. Zotin, Hydroisomerization of n-hexadecane using Pt/alumina-Beta zeolite catalysts for producing renewable diesel with low pour point, Fuel 209 (2017) 521–528, https://doi.org/10.1016/j.fuel.2017.08.011.

[9] D.J. Nowakowski, A.V. Bridgwater, D.C. Elliott, D. Meier, P. de Wild, Lignin fast pyrolysis: results from an international collaboration, J. Anal. Appl. Pyrolysis 88 (2010) 53–72, https://doi.org/10.1016/j.jaap.2010.02.009.

[10] D.C. Elliott, T.R. Hart, Catalytic hydroprocessing of chemical models for bio-oil, Energy Fuels 23 (2009) 631–637, https://doi.org/10.1021/ef8007773.

[11] D.C. Elliott, T.R. Hart, G.G. Neuenschwander, L.J. Rotness, A.H. Zacher, Catalytic hydroprocessing of biomass fast pyrolysis bio-oil to produce hydrocarbon products, Environ. Prog. Sustain. Energy 28 (2009) 441–449, https://doi.org/10.1002/ep.10384.

[12] D.C. Elliott, Historical developments in hydroprocessing bio-oils, Energy Fuels 21 (2007) 1792–1815, https://doi.org/10.1021/ef070044u.

[13] A. Vonortas, N. Papayannakos, Hydrodesulphurization and hydrodeoxygenation of gasoil-vegetable oil mixtures over a Pt/γ-Al2O3catalyst, Fuel Process. Technol. 150 (2016) 126–131, https://doi.org/10.1016/j.fuproc.2016.05.013.

[14] M. Rabaev, M.V. Landau, R. Vidruk-Nehemya, A. Goldbourt, M. Herskowitz, Improvement of hydrothermal stability of Pt/SAPO-11 catalyst in hydro-deoxygenation-isomerization-aromatization of vegetable oil, J. Catal. 332 (2015) 164–176, https://doi.org/10.1016/j.jcat.2015.10.005.

[15] D.C. Elliott, T.R. Hart, G.G. Neuenschwander, L.J. Rotness, M.V. Olarte, A.H. Zacher, Y. Solantausta, Catalytic hydroprocessing of fast pyrolysis bio-oil from pine sawdust, Energy Fuels (2012) 3891–3896, https://doi.org/10.1021/ef3004587.

[16] M.V. Olarte, A.H. Zacher, A.B. Padmaperuma, S.D. Burton, H.M. Job, T.L. Lemmon, M.S. Swita, L.J. Rotness, G.N. Neuenschwander, J.G. Frye, D.C. Elliott, Stabilization of softwood-derived pyrolysis oils for continuous bio-oil hydroprocessing, Top. Catal. 59 (2016) 55–64, https://doi.org/10.1007/s11244-015-0505-7.

[17] A.H. Zacher, M.V. Olarte, D.M. Santosa, D.C. Elliott, S.B. Jones, A review and perspective of recent bio-oil hydrotreating research, Green Chem. 16 (2014) 491–515, https://doi.org/10.1039/c3gc41382a.

[18] D.C. Elliott, E.G. Baker, D. Beckman, Y. Solantausta, V. Tolenhiemo, S.B. Gevert, C. Hörnell, A. Östman, B. Kjellström, Technoeconomic assessment of direct biomass liquefaction to transportation fuels, Biomass 22 (1990) 251–269, https://doi.org/10.1016/0144-4565(90)90021-B.

[19] M. Al-Sabawi, J. Chen, S. Ng, Fluid catalytic cracking of biomass-derived oils and their blends with petroleum feedstocks: a review, Energy Fuels 26 (2012) 5355–5372, https://doi.org/10.1021/ef3006417.

[20] S. Bezergianni, A. Dimitriadis, Comparison between different types of renewable diesel, Renew. Sustain. Energy Rev. 21 (2013) 110–116, https://doi.org/10.1016/j.rser.2012.12.042.

[21] S. Bezergianni, A. Dimitriadis, L.P. Chrysikou, Quality and sustainability comparison of one- vs. two-step catalytic hydroprocessing of waste cooking oil, Fuel 118 (2014) 300–307, https://doi.org/10.1016/j.fuel.2013.10.078.

[22] O.I. Şenol, E.M. Ryymin, T.R. Viljava, A.O.I. Krause, Effect of hydrogen sulphide on the hydrodeoxygenation of aromatic and aliphatic oxygenates on sulphided catalysts, J. Mol. Catal. A Chem. 277 (2007) 107–112, https://doi.org/10.1016/j.molcata.2007.07.033.

[23] E.-M. Ryymin, M.L. Honkela, T.-R. Viljava, A.O.I. Krause, Insight to sulfur species in the hydrodeoxygenation of aliphatic esters over sulfided NiMo/γ-Al2O3 catalyst, Appl. Catal. A Gen. 358 (2009) 42–48, https://doi.org/10.1016/J.APCATA.2009.01.035.

[24] D. Kubička, P. Šimáček, N. Žilková, Transformation of vegetable oils into hydrocarbons over mesoporous-alumina-supported CoMo catalysts, Top. Catal. 52 (2009) 161–168, https://doi.org/10.1007/s11244-008-9145-5.

[25] J.R. Gomes, R.M. Cotta, F. da Silva, R. Oddone, A. de Souza Ferreira, N.F. Fernandes, US 8,366,910 B2, 2013. https://patentimages.storage.googleapis.com/87/51/3c/2fc11b74cadb1b/US8366910.pdf.

[26] G.W. Huber, P. O'Connor, A. Corma, Processing biomass in conventional oil refineries: production of high quality diesel by hydrotreating vegetable oils in heavy vacuum oil mixtures, Appl. Catal. A Gen. 329 (2007) 120–129, https://doi.org/10.1016/j.apcata.2007.07.002.

[27] D. Kubička, J. Horáček, Deactivation of HDS catalysts in deoxygenation of vegetable oils, Appl. Catal. A Gen. 394 (2011) 9–17, https://doi.org/10.1016/j.apcata.2010.10.034.

[28] L.A. Sousa, J.L. Zotin, V. Teixeira Da Silva, Hydrotreatment of sunflower oil using supported molybdenum carbide, Appl. Catal. A Gen. 449 (2012) 105–111, https://doi.org/10.1016/j.apcata.2012.09.030.

[29] F. Wang, J. Xu, J. Jiang, P. Liu, F. Li, J. Ye, M. Zhou, Hydrotreatment of vegetable oil for green diesel over activated carbon supported molybdenum carbide catalyst, Fuel 216 (2018) 738–746, https://doi.org/10.1016/j.fuel.2017.12.059.

[30] S. Phimsen, W. Kiatkittipong, H. Yamada, T. Tagawa, K. Kiatkittipong, N. Laosiripojana, S. Assabumrungrat, Nickel sulfide, nickel phosphide and nickel carbide catalysts for bio-hydrotreated fuel production, Energy Convers. Manage. 151 (2017) 324–333, https://doi.org/10.1016/J.ENCONMAN.2017.08.089.

[31] E. Furimsky, Metal carbides and nitrides as potential catalysts for hydroprocessing, Appl. Catal. A Gen. 240 (2003) 1–28, https://doi.org/10.1016/S0926-860X(02)00428-3.

[32] N. Arun, R.V. Sharma, A.K. Dalai, Green diesel synthesis by hydrodeoxygenation of bio-based feedstocks: strategies for catalyst design and development, Renew. Sustain. Energy Rev. 48 (2015) 240–255, https://doi.org/10.1016/j.rser.2015.03.074.

[33] M. Breysse, G. Djega-Mariadassou, S. Pessayre, C. Geantet, M. Vrinat, G. Pérot, M. Lemaire, Deep desulfurization: reactions, catalysts and technological challenges, Catal. Today 84 (2003) 129–138, https://doi.org/10.1016/S0920-5861(03)00266-9.

[34] J. Han, J. Duan, P. Chen, H. Lou, X. Zheng, Molybdenum carbide-catalyzed conversion of renewable oils into diesel-like hydrocarbons, Adv. Synth. Catal. 353 (2011) 2577–2583, https://doi.org/10.1002/adsc.201100217.

[35] Y. Qin, P. Chen, J. Duan, J. Han, H. Lou, X. Zheng, H. Hong, Carbon nanofibers supported molybdenum carbide catalysts for hydrodeoxygenation of vegetable oils, RSC Adv. 3 (2013) 17485–17491, https://doi.org/10.1039/c3ra42434k.

[36] S. Hollak, Catalytic Deoxygenation of Fatty Acids and Triglycerides for Production of Fuels and Chemicals, (2014) https://dspace.library.uu.nl/bitstream/1874/307935/1/hollak.pdf.

[37] H. Wang, S. Yan, S.O. Salley, K.Y.S. Ng, Hydrocarbon fuels production from hydrocracking of soybean oil using transition metal carbides and nitrides supported on ZSM-5, Ind. Eng. Chem. Res. 51 (2012) 10066–10073, https://doi.org/10.1021/ie3000776.

[38] H. Wang, S. Yan, S.O. Salley, K.Y. Simon Ng, Support effects on hydrotreating of

soybean oil over NiMo carbide catalyst, Fuel 111 (2013) 81–87, https://doi.org/10.1016/j.fuel.2013.04.066.

[39] J. Horáček, Z. Tišler, V. Rubáš, D. Kubička, HDO catalysts for triglycerides conversion into pyrolysis and isomerization feedstock, Fuel 121 (2014) 57–64, https://doi.org/10.1016/j.fuel.2013.12.014.

[40] Z. Tišler, R. Velvarská, L. Skuhrovcová, L. Pelíšková, U. Akhmetzyanova, Key role of precursor nature in phase composition of supported molybdenum carbides and nitrides, Materials (Basel) 12 (2019) 415, https://doi.org/10.3390/ma12030415.

[41] P. Afanasiev, New single source route to the molybdenum nitride Mo2N, Inorg. Chem. 41 (2002) 5317–5319, https://doi.org/10.1021/ic025564d.

[42] Z. Tišler, R. Velvarská, L. Soukupová, J. Horáček, U. Akhmetzyanova, Způsob výroby molybdenového katalyzátoru, CZ 307632 B6, (2019) https://isdv.upv.cz/doc/FullFiles/Patents/FullDocuments/307/307632.pdf.

[43] T. Miyao, I. Shishikura, M. Matsuoka, M. Nagai, S.T. Oyama, Preparation and characterization of alumina-supported molybdenum carbide, Appl. Catal. A Gen. 165 (1997) 419–428, https://doi.org/10.1016/S0926-860X(97)00223-8.

[44] J. Lee, H. Jeon, D.G. Oh, J. Szanyi, J.H. Kwak, Morphology-dependent phase transformation of γ-Al2O3, Appl. Catal. A Gen. 500 (2015) 58–68, https://doi.org/10.1016/j.apcata.2015.03.040.

[45] S. Phimsen, W. Kiatkittipong, H. Yamada, T. Tagawa, K. Kiatkittipong, N. Laosiripojana, S. Assabumrungrat, Nickel sulfide, nickel phosphide and nickel carbide catalysts for bio-hydrotreated fuel production, Energy Convers. Manage. 151 (2017) 324–333, https://doi.org/10.1016/j.enconman.2017.08.089.

[46] M. Al-Sabawi, J. Chen, Hydroprocessing of biomass-derived oils and their blends with petroleum feedstocks: a review, Energy Fuels 26 (2012) 5373–5399, https://doi.org/10.1021/ef3006405.

[47] X. Li, X. Luo, Y. Jin, J. Li, H. Zhang, A. Zhang, J. Xie, Heterogeneous sulfur-free hydrodeoxygenation catalysts for selectively upgrading the renewable bio-oils to second generation biofuels, Renew. Sustain. Energy Rev. 82 (2018) 3762–3797, https://doi.org/10.1016/j.rser.2017.10.091.

[48] R.W. Gosselink, S.A.W. Hollak, S.-W. Chang, J. van Haveren, K.P. de Jong, J.H. Bitter, D.S. van Es, Reaction pathways for the deoxygenation of vegetable oils and related model compounds, ChemSusChem 6 (2013) 1576–1594, https://doi.org/10.1002/cssc.201300370.

[49] M. Anand, A.K. Sinha, Temperature-dependent reaction pathways for the anomalous hydrocracking of triglycerides in the presence of sulfided Co–Mo-catalyst, Bioresour. Technol. 126 (2012) 148–155, https://doi.org/10.1016/j.biortech.2012.08.105.

[50] S.K. Kim, J.Y. Han, H. Shik Lee, T. Yum, Y. Kim, J. Kim, Production of renewable diesel via catalytic deoxygenation of natural triglycerides: comprehensive understanding of reaction intermediates and hydrocarbons, Appl. Energy 116 (2014) 199–205, https://doi.org/10.1016/j.apenergy.2013.11.062.